

# SUPERGRANULATION AS THE LARGEST BUOYANTLY DRIVEN CONVECTIVE SCALE OF THE SUN

JEAN-FRANCOIS COSSETTE

Laboratory for Atmospheric and Space Physics, University of Colorado, Boulder, USA

MARK P. RAST

Department of Astrophysical and Planetary Sciences, Laboratory for Atmospheric and Space Physics, University of Colorado, Boulder, USA

*Draft version June 14, 2016*

## ABSTRACT

Supergranulation is characterized by horizontally divergent flows with typical length scales of 32 Mm in the solar photosphere. Unlike granulation, the size of which is comparable to both the thickness of the radiative boundary layer and local scale height of the plasma in the photosphere, supergranulation does not reflect any obvious length scale of the solar convection zone. Early suggestions that the depth of second helium ionization is important are not supported by numerical simulations. Thus the origin of the solar supergranulation remains largely a mystery. Moreover, observations of flows in the photosphere using either Doppler imaging or correlation or feature tracking show a monotonic decrease in power at scales larger than supergranulation. Both local area and global spherical shell simulations of solar convection by contrast show the opposite, a power law increase in horizontal flow amplitudes to low wavenumber. Here we examine this disparity, and investigate how the solar supergranulation may arise as a consequence of strong photospheric driving and non-local heat transport by cool diving plumes. Using three dimensional anelastic simulations with surface driving, we show that the kinetic energy of largest convective scales in the upper layers of a stratified domain reflects the depth of transition from strong buoyant driving to adiabatic stratification below. We interpret the observed monotonic decrease in solar convective power at scales larger than supergranulation to be a consequence of this rapid transition, and show how the supergranular scale can be understood as the largest buoyantly driven mode of convection in the Sun.

*Subject headings:* Sun: interior

## 1. INTRODUCTION

Scales of solar convection fall into three main categories, granules, mesogranules and supergranules, with recent observations hinting at the possibility of giant cells (Hathaway et al. 2013). Granules (1Mm diameter, 0.2 hr lifetime) are the signature of convective cells driven in the highly superadiabatic layers of the photosphere. Direct observation in continuum intensity images has confirmed their convective nature via the correlation of vertical velocity with intensity (e.g. Nordlund et al. (2009)). Supergranules (32Mm diameter; 1.8 day lifetime) are observed largely as a horizontal flow using either Doppler imaging, magnetic feature or granule tracking, or local helioseismology (Hanasoge et al. 2016). The horizontally divergent motion and cellular nature of supergranulation suggest a convective origin. The presence of magnetic flux elements in network boundaries makes direct observation of the vertical velocity and intensity correlation difficult, though the temperature contrast across the cells has been measured (Goldbaum et al. 2009). The physical mechanism responsible for supergranulation remains unclear. The early suggestion that the second ionization of helium plays an important role (Leighton et al. 1962; Simon & Leighton 1964; November et al. 1981) is not supported by numerical simulation (Rast & Toomre 1993; Lord et al. 2014), while the later suggestion that supergranulation results from self-organization of granular flows (Rieutord et al. 2000; Rast 2003; Crouch et al. 2007) may be more relevant on mesogranular scales (Cattaneo et al. 2001; Berrilli et al. 2005; Leitzinger et al. 2005; Duvall & Birch 2010). Mesogranules (5Mm diameter; 3 hour lifetime) are intermediate scale structures seen primarily as vertical velocity in time-averaged

Doppler maps (November et al. 1981). Their existence as a real convective feature distinct from both granules and supergranules is still debated (November 1989; Berrilli et al. 2013).

Convective structures much larger than supergranules, including so-called giant cells, are predicted by both mixing length theories and global models of solar convection (Christensen-Dalsgaard et al. 1996; Miesch et al. 2008). However, observations suggest that the velocities associated with these large-scale flow motions are significantly weaker than predicted. Time distance helioseismology provides the most severe constraint, with large-scale velocity amplitudes at 28-56Mm depth measured to be orders of magnitude smaller than in models (Hanasoge & Sreenivasan 2014; Hanasoge et al. 2012, 2010). However, ring diagram helioseismic analysis does not confirm this, instead showing at 30Mm depth a continuous increase of power to scales larger than supergranulation, in good agreement with numerical experiments (Greer et al. 2015). Where models and observations most fundamentally disagree is in the surface layers. Horizontal velocity power spectra obtained from Doppler imaging and correlation tracking of flow features at the solar surface reveal peaks corresponding to granular (angular harmonic degree  $l \sim 3500$ ) and supergranular scales ( $l \sim 120$ ), followed by a monotonic decrease in power to larger scales (Hathaway et al. 2000; Roudier et al. 2012; Hanasoge & Sreenivasan 2014; Hathaway et al. 2015). Only recently has a possible signature of giant cell convection been detected in the photosphere by carefully tracking the motions of supergranules (Hathaway et al. 2013). Radiative hydrodynamic and magnetohydrodynamic local area and global models of solar convection, on the other hand, all show horizon-

tal power increasing monotonically to large scales (Lord et al. 2014; Hanasoge et al. 2016).

This discrepancy between modeled and observed power may be related to the difficulties global models have reproducing a solar-like differential rotation in the parameter regime characteristic of the solar interior. Models indicate that rotationally constrained giant cells, which transport angular momentum toward the equator, are essential in maintaining the prograde equatorial differential rotation (e.g. Miesch et al. (2008)) observed at the photosphere and in accordance with the angular velocity profiles inferred from helioseismology (Thompson et al. 2003). These solar-like states are achieved when the flow is rotationally constrained, when the influence of the Coriolis force dominates over the flow's inertia, which places an upper limit on the convective flow speeds. This upper limit is weaker than the flow amplitudes required to transport the solar luminosity in global simulations (e.g. Hotta et al. (2015)). Moreover, as numerical diffusivities are lowered, the flows become more turbulent and velocity fields tend to decorrelate, which can lead to faster convective motions and retrograde differential rotation (poles rotating faster than the equator) instead of prograde (Gastine et al. 2013; Featherstone & Miesch 2015). Models of the Sun's convection can reproduce global scale motions only if the flux through the domain is reduced or the rotation rate of the star is increased.

These difficulties suggest that global motions in the Sun are weak enough to be rotationally constrained, with smaller scales carrying the convective flux. This is possible if the Sun maintains a mean gradient in the deep convection zone that is closer to adiabatic than that achievable in most simulations and dissipative effects are negligible, limiting convective driving below the surface and leading to a horizontal velocity spectrum in the photosphere consistent with that observed (Lord et al. 2014). It implies that the solar supergranulation reflects the largest buoyantly driven convective scale of the Sun.

In this paper we use 3D numerical simulations of solar convection to assess this possibility. We do this by vigorously driving surface convection in the upper layers while simultaneously achieving a nearly adiabatic stratification in the interior. We examine the spectra that result and show that they are dependent on the rate of the transition to adiabatic stratification. We show that, when the transit time of the fluid parcels across the convection zone is much shorter than the diffusion time, the depth over which this transition takes place depends only on the change in the filling factor of the downflows with depth due to stratification.

## 2. MODEL

We simulate solar hydrodynamic convection by solving the Lipps & Hemler (Lipps & Hemler 1982) version of the anelastic Euler equations governing the evolution of momentum and entropy perturbations in a gravitationally stratified fluid:

$$\frac{D\mathbf{u}}{Dt} = -\nabla\pi' + g\frac{\Theta'}{\Theta_o}\mathbf{k}, \quad (1)$$

$$\frac{D\Theta'}{Dt} = -\mathbf{u} \cdot \nabla\Theta_a - \frac{\Theta'}{\tau}, \quad (2)$$

$$\nabla \cdot (\rho_o \mathbf{u}) = 0. \quad (3)$$

Here,  $\mathbf{u}$  represents the fluid velocity,  $\Theta \equiv \Theta' + \Theta_a$  is the potential temperature (equivalent to the specific entropy since

$ds = c_p d \ln \Theta$ , with  $c_p$  the specific heat at constant pressure), and  $\pi' \equiv p'/\rho_o$  is the density-normalized pressure perturbation.

The *reference* state about which the anelastic asymptotic expansion is constructed is denoted by the subscript 'o'. It is taken as isentropic (i.e.  $\Theta_o = \text{constant}$ ) and in hydrostatic balance, with  $g(r) = g_b(r_b/r)^{-2}$  the radially-diminishing magnitude of gravity acceleration pointing in the negative unit vector direction  $\mathbf{k}$ . The reference state is constructed using values for temperature  $T_b$ , density  $\rho_b$  and gravitational acceleration  $g_b$  at the base of the domain obtained from a solar structure model (Christensen-Dalsgaard et al. 1996).

Primes in equations (1) and (2) denote perturbations with respect to an arbitrarily selected *ambient* state (denoted by the subscript 'a'). The ambient state chosen here represents the large scale thermodynamic equilibrium structure of the Sun on time scales much longer than the convective turnover time  $\tau_c$ . The Newtonian cooling term,  $-\Theta'/\tau$ , in (2) relaxes the potential temperature to that of the ambient state over a time scale  $\tau \gg \tau_c$ . Thus the ambient entropy stratification of the domain is maintained over long time scales, limiting restratification by the convection and driving motions in regions of superadiabaticity. This is a common approach in atmospheric models when addressing evolutionary fluctuations about large scale equilibria (Smolarkiewicz et al. 2001; Grabowski & Smolarkiewicz 2002; Warn-Varnas et al. 2007) and has also been employed in some previous simulations of global solar magneto-convection (Ghizaru et al. 2010; Racine et al. 2011; Cossette et al. 2013).

In detail, we construct the ambient state to be strongly subadiabatic in the lower portion of the computational domain  $r_b \leq r < r_i$ , with  $r_i = 0.718R_\odot$ , adiabatic in the bulk  $r_i \leq r \leq r_s$ , with the value of  $r_s$  varying between runs, and superadiabatic above  $r_s < r \leq r_t$ . It satisfies the polytropic equations for an ideal gas,  $p_a = K\rho_a^{1+1/m}$ ,  $p_a = \rho_a R T_a$ , and  $dp_a/dr = -\rho_a g$  with a prescribed polytropic index  $m = m(r)$ . In the subadiabatic lower portion of the domain the polytropic index  $m$  decreases linearly from  $m_b = 3.0$  at the base to  $m_i = m_{ad} = 3/2$  at  $r = r_i$ . It then remains constant at its adiabatic value through the bulk of the domain, before being set to a superadiabatic value  $m_s < m_{ad}$  above  $r = r_s$ . The index  $m_s$  thus specifies the level of superadiabaticity in the region  $r > r_s$ , with the thickness and superadiabaticity of the upper region differing between simulation runs. The ambient potential temperature profile for each run is then  $\Theta_a \equiv T_a(\rho_b T_b / \rho_a T_a)^{1-1/\gamma}$ .

The relaxation time to the ambient state is set to  $\tau = 20$  solar days in the stably stratified and superadiabatic regions and  $\tau = 1000$  solar days in the adiabatic bulk of the domain. It is important to note that, while we call the bulk of the domain adiabatic, this is a statement about the ambient state only. The long relaxation time in that portion allows the convection to reconfigure the thermodynamic gradients therein. This allows us to study how the interior of the convection zone (CZ) evolves when subject to strong surface driving and how this in turn effects the spectrum of the motions that ensue. As a control experiment, we also consider a simulation for which the ambient state is subadiabatic in the lower portion  $r_b \leq r < r_i$  (as described above) but weakly superadiabatic across the remainder of the domain  $r_i \leq r < r_t$ . The relaxation time in that case is taken to be 20 solar days throughout.

Integration of (1)-(3) is carried out with the hydrodynamic solver of the magnetohydrodynamic EULAG

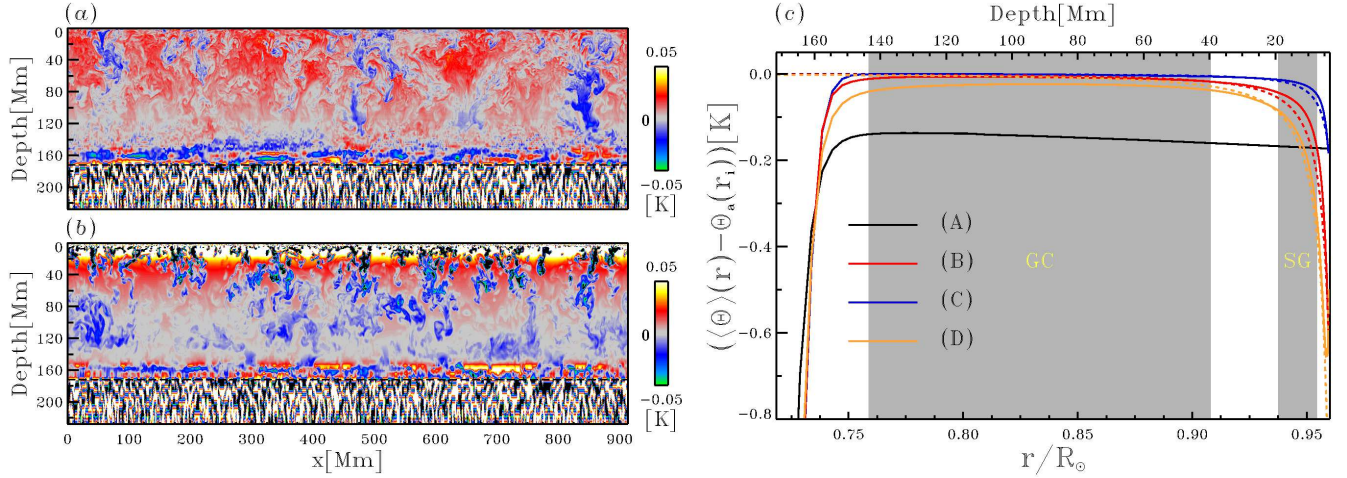


FIG. 1.— Vertical cross-sections of the instantaneous deviations  $\tilde{\Theta} \equiv \Theta - \langle \Theta \rangle$  from the horizontal mean of the PT  $\langle \Theta \rangle$  taken from case A—panel (a) and B—panel (b). Case A is characterized by a weakly superadiabatic ambient profile ( $m_s = 1.4999998$ ) across the full depth of the CZ ( $r_t \geq r \geq r_i$ ), whereas case B uses a strictly adiabatic profile in the region ( $r_s \geq r \geq r_i$ ,  $r_s \equiv 0.96R_\odot$ ) and a superadiabatic profile ( $m_s = 1.4994$ ) inside a 3.5Mm deep region below the surface ( $r_t \geq r \geq r_s$ ). The horizontal dashed line denotes the location of the core-envelope interface. Low entropy fluid parcels produced in the driven region pass through the convecting layer and impact the stable layer below, exciting gravity waves there. Panel (c) shows profiles of  $\langle \Theta(r) \rangle - \Theta_a(r_i)$  for each case in the region  $r_s \geq r \geq r_i$  (solid lines). As Case B, Cases C and D use, respectively, strictly adiabatic ambient profiles below  $r_s = 0.96R_\odot$  and superadiabatic profiles characterized by  $m_s = 1.49985$  and  $m_s = 1.4985$  in the region above. Shaded areas labeled ‘GC’ and ‘SG’ correspond to depth ranges over which  $100\text{Mm} < 4H_\rho < 300\text{Mm}$  and  $20\text{Mm} < 4H_\rho < 50\text{Mm}$ , respectively. The change in the mean stratification near the surface in Cases B-D is well reproduced by cold fluid parcels moving down adiabatically from the height  $r_s$  at which they originate:  $\langle \Theta(r) \rangle - \Theta_a(r_i) \approx f(r)\Theta_d$ , where  $\Theta_d$  is the parcels’ average potential temperature at  $r = r_s$  and  $f(r) \equiv f_d\rho_o(r_s)/\rho_o(r)$  is their filling factor, with  $f_d$  the filling factor of downflows at  $r = r_s$  (see dashed lines). The accumulation of low entropy fluid near the base of the CZ causes  $\langle \Theta(r) \rangle$  to decrease very rapidly in that region.

model (Prusa et al. 2008; Smolarkiewicz & Charbonneau 2013). EULAG employs a two-time-level flux-form Eulerian non-oscillatory forward-in-time advection operator (Smolarkiewicz 2006), allowing stable integration of the equations with all dissipation delegated to the advection scheme’s truncation terms (Smolarkiewicz & Prusa 2002). We examine a Cartesian domain extending from  $r_b = 0.63R_\odot$  to  $r_t = 0.965R_\odot$  in solar radius, which has physical dimensions  $910.53\text{Mm} \times 910.53\text{Mm} \times 227.63\text{Mm}$  on grids of  $1024^2 \times 256$  points. The reference states are characterized by density scale heights  $H_\rho = 360\text{km}$  at the surface and  $85\text{Mm}$  at the base, spanning a total of eleven scale heights across the domain. Nonuniform gridding in the vertical direction accommodates the rapidly decreasing density scale-height near the top of the domain (Prusa & Smolarkiewicz 2003). The domain is horizontally periodic, with vanishing vertical velocity, stress-free horizontal velocity, and zero flux of the potential temperature imposed at both upper and lower boundaries.

### 3. RESULTS

First we compare two simulations which share approximately the same convective flux through the bulk of the domain. In Case A we specify a weakly superadiabatic ambient state across the full depth of the layer while in Case B the strongly superadiabatic ambient state is confined to a 3.5Mm deep region below the surface (hereafter, the cooling layer). The typical spatial scale of the low entropy parcels generated in the cooling layer reflects the turbulent energy injection scale  $L \sim 4H_\rho$  in this region ( $H_\rho \sim 0.36 - 2.6\text{Mm}$ ) (Rincon 2007; Lord et al. 2014). As can be seen from Figure 1, the flow in Case A is dominated by larger scale motions than Case B. In particular, positive entropy perturbations in Case A, although weaker, tend to be coherent over the full depth of the convection zone (Fig. 1a).

To understand the physical processes shaping the flow structure we consider additional experiments with different

values of the polytropic index  $m_s$  in the cooling layer (Cases C & D). The mean thermodynamic stratification (Fig. 1c) in Case A is characterized by a weakly superadiabatic mean state ( $d\langle \Theta \rangle / dr < 0$ ) throughout. Cases B-D, on the other hand, show mean states very close to adiabatic throughout the bulk but strongly superadiabatic near the surface. The turbulent energy injection scale in this region is comparable to the size of supergranules (region SG in Fig. 1c). The strong buoyancy force therein thus drives upflows on the scale of supergranulation (red and yellow areas in Fig. 1b). The convectively unstable mean stratification through the bulk of the CZ in Case A (‘GC’ region in Fig. 1c), on the other hand, additionally drives giant cell scale motions.

It is important to note that, while in Case A the superadiabatic mean entropy profile is maintained by relaxation to the superadiabatic ambient state, the relaxation time in Cases B-D is too long to be important in determining the mean stratification. The strongly superadiabatic region below the cooling layer is caused by the presence of the cool downflowing plumes which change the mean state, driving the upflows. This effect decreases with depth because the filling factor of the downflows decreases with increasing density until their effect on the mean state becomes negligible. In all Cases B-D, parcels originate from the same depth but have different initial entropy fluctuations. The downflowing fluid in cases with larger entropy fluctuations must achieve smaller filling factors before their influence on the mean state becomes negligible, hence the increase of the extent of the superadiabatic region when comparing Case C to B, and B to D. Note that the transit time  $\tau_t$  of the cool plumes across the simulated CZ ( $\tau_t \approx 1$  solar day) is shorter than the time it takes for a parcel to diffuse numerically. As a result, the change in the mean stratification below the surface is well approximated by parcels moving adiabatically across the layer (see dashed lines in Fig. 1c).

In the Sun, radiative diffusion dominates over conduction,



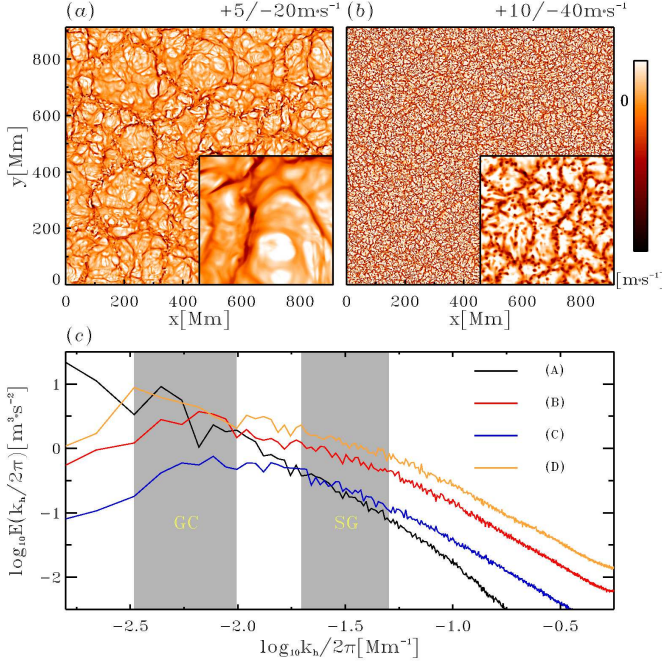


FIG. 2.— Horizontal cross-sections of the instantaneous vertical velocity  $u_r$  taken at 5Mm depth corresponding to Cases A—panel (a) and B—panel (b). The inserted plot in each panel shows the magnified view of a  $100 \text{ Mm}^2$  area. As in other experiments of compressible convection,  $u_r$  is characterized by broad upflows surrounded by a network of narrow downflow lanes (see Nordlund et al. (2009), Miesch & Toomre (2009) and references therein). Panel (c): Horizontal velocity power spectra taken at 5Mm depth for each case. Here,  $k_h \equiv 2\pi/\lambda$ , with  $\lambda$  the horizontal wavelength. Shaded areas labeled ‘GC’ and ‘SG’ correspond, respectively, to regions where  $100 \text{ Mm} < \lambda < 300 \text{ Mm}$  (hereafter, giant cells) and  $20 \text{ Mm} < \lambda < 50 \text{ Mm}$  (hereafter, supergranular scales).

with estimates for the radiative diffusivity ranging between  $\kappa \sim 10^5 - 10^7 \text{ cm}^2 \cdot \text{s}^{-1}$  (Miesch 2005). The characteristic diffusion timescale  $\tau_d \sim l^2/\kappa$  of a plume with spatial scale  $l \sim 300 \text{ km}$  (i.e. the thickness of the radiative boundary layer at the photosphere) is thus between 3–285yr. Assuming that the transit time  $\tau_t$  of cold plumes generated at the photosphere is of order the turnover time of the largest convective cells ( $\sim 1$  month),  $\tau_t \ll \tau_d$ . Solar plumes may then be expected to behave as in Cases B–D, travelling across the convection zone without exchanging a significant amount of heat with the surrounding medium. The consequent superadiabatic mean solar stratification is due only to the plumes’ presence and their geometry as they move across layers of increasing density. This implies that the interior stratification of the Sun could be extremely close to adiabatic with a relatively thin superadiabatic layer determined by the thermodynamic properties of the granular downflows in the upper layers.

The characteristic scales of the convective flows reflect the depth of the superadiabatic region. Cell diameters in Case A are much larger than in Case B, with  $200 \text{ Mm}$  scales typical in Case A and smaller  $40 \text{ Mm}$  scales in Case B (Fig. 2a and b). This difference is reflected in the horizontal velocity power spectra of the flows (Fig. 2c). At 5Mm depth, the power contained in supergranular scales in Case B exceeds that of Case A, whereas the opposite is true of the power at the largest giant-cell scales. Increasing the polytropic index  $m_s$  in the cooling layer of Case C decreases the power at all scales relative to Case B, while decreasing it in Case D increases the amplitude of the convective motions (Fig. 2c).

Notably, the increase of power due to the intensification of

Case	$P_G/P_{G_A}$	$P_S/P_{S_A}$	$P_S/P_G$	$\epsilon_G$ [ $\times 10^{-8}$ ]	$\epsilon_S$ [ $\times 10^{-8}$ ]	d [Mm]
A	1.0000	1.0000	0.2241	-1.68	-0.25	-
B	0.7082	3.5573	1.1255	-0.86	-11.1	30.5
C	0.1385	1.1654	1.8857	-0.23	-3.0	12.5
D	1.2807	6.0726	1.0625	-1.15	-20.6	41.8

TABLE 1

RELATIONSHIP BETWEEN THE HORIZONTAL POWER DISTRIBUTION AT 5MM DEPTH AND THE SUPERADIABATICITY OF THE CONVECTION ZONE. SECOND AND THIRD COLUMNS SHOW, RESPECTIVELY, THE TOTAL POWER CONTAINED IN GIANT CELLS ( $P_G$ ) AND SUPERGRANULAR SCALES ( $P_S$ ) RELATIVE TO THAT OF CASE A, WITH THE FOURTH COLUMN SHOWING THE RATIO OF SUPERGRANULAR TO GIANT CELL POWER. FIFTH AND SIXTH COLUMNS DISPLAY, RESPECTIVELY, THE MAXIMAL VALUE OF THE SUPERADIABATICITY PARAMETER  $\epsilon \equiv H_T/\Theta_o d\langle\Theta\rangle/dr$  INSIDE DRIVING REGIONS CORRESPONDING TO GIANT CELLS ( $100 \text{ Mm} < 4H_p < 300 \text{ Mm}$ ) AND SUPERGRANULAR SCALES ( $20 \text{ Mm} < 4H_p < 50 \text{ Mm}$ ), WITH  $H_T \equiv -(d \ln T_o/dr)^{-1}$  THE TEMPERATURE SCALE HEIGHT. THE LAST COLUMN SHOWS THE CHARACTERISTIC DEPTH OF THE SUPERADIABATIC REGION BELOW THE SURFACE FOR CASES B–D (ESTIMATED AS THE SMALLEST DEPTH FOR WHICH  $\epsilon \leq 10^{-8}$ ).

convective driving, when going from Case C to Case B and then from Case B to Case D, is accompanied by a corresponding increase of the spatial extent of the superadiabatic region below the surface (Fig. 1c). The power contained in giant cells in Cases B–D relative to Case A ( $P_G/P_{G_A}$ ) increases with the superadiabaticity of the GC region ( $\epsilon_G$ ), as summarized in Table 1. The table also shows the correlation between the power contained in the supergranular scales ( $P_S/P_{S_A}$ ) and the superadiabaticity of the SG region ( $\epsilon_S$ ). The ratio of supergranular to giant cell power ( $P_S/P_G$ ) is the largest in Case C, where the rate of transition to adiabatic stratification is the greatest and the characteristic depth (d) of the superadiabatic region is the smallest.

#### 4. SUMMARY & REMARKS

These surface driven convective experiments demonstrate that low entropy fluid parcels generated in a cooling layer can lead to a mean thermodynamic state that is strongly superadiabatic in a narrow region, smoothly transitioning to very nearly adiabatic stratification below, much more adiabatic than has been achieved by other simulations to date. The depth of the superadiabatic region depends on the entropy contrast and density of the downflowing plumes, and the convective modes of that layer then determine the velocity power spectrum observed (Lord et al. 2014).

Cold fluid parcels generated in the cooling layer transit the convection zone over a time short compared to numerical diffusion timescales. Thus the stratification of the upper convection zone is well approximated by the contribution adiabatically descending cool parcels make to the mean state strictly by their presence. The filling factor of the downflows decreases with the increasing mean density, yielding, because of the steep stratification, a nearly adiabatic profile at depth. The ratio of power at supergranular to giant cell scales reflects this, increasing in those simulations with a shallower transition to adiabatic stratification.

The short transit time of the cold downflowing plumes across the solar convection zone compared to the characteristic timescale of radiative heating in the solar interior suggests that heat transport is highly non-local (e.g. Spruit (1997)). Similar to our simulations, the change in the mean stratifi-

cation of the upper solar convection zone then reflects the plumes' presence and the decrease in their filling factor with depth, as opposed to diffusive processes, which are minimized in our solutions and likely insignificant in the Sun. The solar supergranulation then reflects density scale height at the depth at which the solar mean state becomes essentially isentropic. This is quite shallow because of the low density of the granular downflows and the rapid increase in the mean density of the subphotospheric layers, increasing by a factor of  $\sim 1.5 \times 10^4$  in the upper 20Mm. If this picture is correct, supergranulation represents the largest buoyantly driven con-

vective scale of the Sun.

#### ACKNOWLEDGEMENTS

We thank Regner Trampedach, Axel Brandenburg, and Piotr Smolarkiewicz. This work utilized the Janus supercomputer, supported by the National Science Foundation (award number CNS-0821794) and the University of Colorado Boulder. The Janus supercomputer is a joint effort of the University of Colorado Boulder, the University of Colorado Denver and the National Center for Atmospheric Research. J.-F.C. acknowledges support from the University of Colorado's George Ellery Hale Postdoctoral Fellowship. M.P.R.'s work was partially supported by NASA award NNX12AB35G.

#### REFERENCES

- Berrilli, F., Del Moro, D., Russo, S., Consolini, G., & Straus, T. 2005, *ApJ*, 632, 677
- Berrilli, F., Scardigli, S., & Giordano, S. 2013, *Sol. Phys.*, 282, 379
- Cattaneo, F., Lenz, D., & Weiss, N. 2001, *ApJ*, 563, L91
- Christensen-Dalsgaard, J., Dappen, W., Ajukov, S. V., et al. 1996, *Science*, 272, 1286
- Cossette, J.-F., Charbonneau, P., & Smolarkiewicz, P. K. 2013, *ApJ*, 777, L29
- Crouch, A. D., Charbonneau, P., & Thibault, K. 2007, *ApJ*, 662, 715
- Duvall, T. L., Jr., & Birch, A. C. 2010, *ApJ*, 725, L47-L51
- Featherstone, N. A., & Miesch, M. S. 2015, *ApJ*, 804, 67
- Gastine, T., Wicht, J., & Aurnou, J. M. 2013, *Icarus*, 225, 156
- Ghizaru, M., Charbonneau, P., & Smolarkiewicz, P. K. 2010, *ApJ*, 715, L133
- Goldbaum, N., Rast, M. P., Ermolli, I., Sands, J. S., & Berrilli, F. 2009, *ApJ*, 707, 67
- Grabowski, W. W., & Smolarkiewicz, P. K. 2002, *Monthly Weather Review*, 130, 939
- Greer, B. J., Hindman, B. W., Featherstone, N. A., & Toomre, J. 2015, *ApJ*, 803, L17
- Hanasoge, S. M., Duvall, T. L., Jr., & DeRosa, M. L. 2010, *ApJ*, 712, L98
- Hanasoge, S. M., Duvall, T. L., & Sreenivasan, K. R. 2012, *Proceedings of the National Academy of Science*, 109, 11928
- Hanasoge, S. M., & Sreenivasan, K. R. 2014, *Sol. Phys.*, 289, 3403
- Hathaway, D. H., Beck, J. G., Bogart, R. S., et al. 2000, *Sol. Phys.*, 193, 299
- Hathaway, D. H., Teil, T., Norton, A. A., & Kitiashvili, I. 2015, *ApJ*, 811, 105
- Hathaway, D. H., Upton, L., & Colegrove, O. 2013, *Science*, 342, 1217
- Hotta, H., Rempel, M., & Yokoyama, T. 2015, *ApJ*, 803, 42
- Leighton, R. B., Noyes, R. W., & Simon, G. W. 1962, *ApJ*, 135, 474
- Leitzinger, M., Brandt, P. N., Hanslmeier, A., Pötzi, W., & Hirzberger, J. 2005, *A&A*, 444, 245
- Lipps, F. B., & Hemler, R. S. 1982, *Journal of Atmospheric Sciences*, 39, 2192
- Lord, J. W., Cameron, R. H., Rast, M. P., Rempel, M., & Roudier, T. 2014, *ApJ*, 793, 24
- Miesch, M. S. 2005, *Living Reviews in Solar Physics*, 2, 1
- Miesch, M. S., Brun, A. S., De Rosa, M. L., & Toomre, J. 2008, *ApJ*, 673, 557
- Miesch, M. S., & Toomre, J. 2009, *Annual Review of Fluid Mechanics*, 41, 317
- Nordlund, Å., Stein, R. F., & Asplund, M. 2009, *Living Reviews in Solar Physics*, 6, 2
- November, L. J., Toomre, J., Gebbie, K. B., & Simon, G. W. 1981, *ApJ*, 245, L123
- November, L. J. 1989, *ApJ*, 344, 494
- Prusa, M. P., & Smolarkiewicz, P. K. 2003, *Journal of Computational Physics*, 190, 601
- Prusa, J. M., Smolarkiewicz, P. K., & Wyszogrodzki, A. A. 2008, *Comput. Fluids*, 37, 1193
- Racine, É., Charbonneau, P., Ghizaru, M., Bouchat, A., & Smolarkiewicz, P. K. 2011, *ApJ*, 735, 46
- Rast, M. P. 2003, *ApJ*, 597, 1200
- Rast, M. P., & Toomre, J. 1993, *ApJ*, 419, 224
- Rincon, F. 2007, *IAU Symposium*, 239, 58
- Rieutord, M., Roudier, T., Malherbe, J. M., & Rincon, F. 2000, *A&A*, 357, 1063
- Roudier, T., Rieutord, M., Malherbe, J. M., et al. 2012, *A&A*, 540, A88
- Simon, G. W., & Leighton, R. B. 1964, *ApJ*, 140, 1120
- Smolarkiewicz, P. K., Margolin, L. G., & Wyszogrodzki, A. A. 2001, *Journal of Atmospheric Sciences*, 58, 349
- Smolarkiewicz, P. K. 2006, *International Journal for Numerical Methods in Fluids*, 50, 1123
- Smolarkiewicz, P. K., & Charbonneau, P. 2013, *Journal of Computational Physics*, 236, 608
- Smolarkiewicz, P. K., & Prusa, J. M. 2002, *International Journal for Numerical Methods in Fluids*, 39, 799
- Spruit, H. 1997, *Mem. Soc. Astron. Italiana*, 68, 397
- Thompson, M. J., Christensen-Dalsgaard, J., Miesch, M. S., & Toomre, J. 2003, *ARA&A*, 41, 599
- Warn-Varnas, A., Hawkins, J., Smolarkiewicz, P. K., et al. 2007, *Ocean Modelling*, 18, 97